Analysis of the Myc-induced pancreatic β cell islet tumor microenvironment using imaging ToF-SIMS

Blake M. Bluestein,[1] Fionnuala Morrish,[2] Daniel J. Graham,[1] Li Huang,[2] David Hockenbery,[2] and Lara J. Gamble[1,a]
[1]Department of Bioengineering, University of Washington, Seattle, Washington 98195
[2]Fred Hutchinson Cancer Research Center, Seattle, Washington 98109

Solid tumors are a structurally complex system, composed of many different cell types. The tumor microenvironment includes nonmalignant cell types that participate in complex interactions with tumor cells. The cross talk between tumor and normal cells is implicated in regulating cell growth, metastatic potential, and chemotherapeutic drug resistance. A new approach is required to interrogate and quantitatively characterize cell to cell interactions in this complex environment. Here, the authors have applied time-of-flight secondary ion mass spectrometry (ToF-SIMS) to analyze Myc-induced pancreatic β cell islet tumors. The high mass resolution and micron spatial resolution of ToF-SIMS allows detection of metabolic intermediates such as lipids and amino acids. Employing multivariate analysis, specifically, principal component analysis, the authors show that it is possible to chemically distinguish cancerous islets from normal tissue, in addition to intratumor heterogeneity. These heterogeneities can then be imaged and investigated using another modality such as sum harmonic generation microscopy. Using these techniques with a specialized mouse model, the authors found significant metabolic changes occurring within β cell tumors and the surrounding tissues. Specific alterations of the lipid, amino acid, and nucleotide metabolism were observed, demonstrating that ToF-SIMS can be utilized to identify large-scale changes that occur in the tumor microenvironment and could thereby increase the understanding of tumor progression and the tumor microenvironment. *Published by the AVS.* https://doi.org/10.1116/1.5038574

I. INTRODUCTION

Solid tumors are a structurally complex system consisting of tumor cells, infiltrating immune cells, and nonmalignant stromal cells. The physical and chemical interactions between malignant cells and nontransformed cells create the tumor microenvironment. This environment has been implicated in the regulation of cell growth, determining metastatic potential, and impacting the outcome of chemotherapy.[1,2] Tumor growth depends on the conversion of nutrients into biochemical and biosynthetic precursors especially within lipid pathways, as lipids are used for cell membrane formation, signaling, and energy. However, these metabolic requirements are impacted by the tumor microenvironment, which determines the availability of nutrients such as glucose and glutamine, and oxygen supplied to the tumor.[3]

The use of an inducible *c-Myc* oncogene in a well-established model of pancreatic β cell tumorigenesis provides a controlled system in which to observe β cell tumorigenesis and investigate the role of the tumor microenvironment in tumor growth.[4] Myc, a transcription factor, is one of the most frequently deregulated oncogenes in human cancers.[5] Deregulation of Myc is responsible for many of the metabolic changes that induce malignancy. Myc deregulation alters glucose, glutamine, and lipid metabolism and significantly modifies mitochondrial function.[6–11] While it is

known that Myc is frequently deregulated in many cancers, it is unknown how Myc-activated tumor metabolism is impacted by an adjacent cellular environment that has the potential to either assist or restrict the tumor growth. Many biochemical processes that contribute to tumor initiation and growth could be affected by the synthesis or degradation of specific metabolites ranging from nucleotides and lipids to amino acids within the tumor microenvironment. Chemical imaging of Myc pancreatic tissues with micron resolution would permit the assessment of endogenous cellular metabolic products within specific β cell tumor regions and surrounding tissue (made up of acinar cells). Harnessing the capabilities of high resolution chemical imaging allows for the development of methods to evaluate how these distinct tissue regions affect each other's metabolism, further aiding our understanding of the tumor microenvironment.

Metabolic analyses require sensitivity, specificity, selectivity, and speed, which are strengths of utilizing mass spectrometry imaging (MSI) as an optimal technique to detect and identify biologically relevant metabolites.[12–16] Imaging time-of-flight secondary ion mass spectrometry (ToF-SIMS) provides detailed spatial ($<2\,\mu$m) and chemical information providing a new perspective to biological tissue analysis that has not been available using techniques commonly used for clinically relevant samples, such as high-performance liquid chromatography, fluorescent microscopy, and immunohistochemistry.[17,18] Recent chemical imaging research using a Myc-driven mouse model of

a)Electronic mail: lgamble@uw.edu

renal cell carcinoma demonstrated that glutamine-derived lipids and metabolites drive tumor progression.[19] Further chemical imaging research using a Myc model of lung adenocarcinoma also showed that tumors have distinct lipid signatures compared with normal tissue.[20] These studies were conducted using entire cancerous kidney or lung sections, but individual Myc-induced pancreatic islet tumors have yet to be explored in this manner.

The objective of this work is to use ToF-SIMS to map and identify molecules associated with the metabolic changes induced by Myc overexpression in pancreatic β cell tumors and the adjacent cellular environment in the *pIns-MycER^{TAM}/p53$^{-/-}$* mouse model with Myc-inducible pancreatic β cell tumorigenesis. In this model, the induction of Myc promotes rapid tumorigenesis, with tumors occupying the majority of the pancreas within 12 days; for this reason, we chose to study the 6 day stage where there is evident hyperplasia and a distinct exocrine tissue available for analysis. Imaging ToF-SIMS and principal component analysis (PCA) are used to identify, map, and compare chemical differences within Myc-induced islet tumors and surrounding acinar cells after 6 days of Myc activation with tamoxifen in the *pIns-MycER^{TAM}/p53$^{-/-}$* mouse model (referred to hereafter as Myc tissues). Pancreatic islets from p53$^{-/-}$ mice, also treated with tamoxifen, are used as controls (hereafter referred to as control tissue). In this work, we provide evidence of significant metabolic changes occurring within Myc-driven β cell tumors and the surrounding tissue by combining sophisticated animal models with imaging ToF-SIMS. We also demonstrate the application of ToF-SIMS and sum harmonic generation (SHG) microscopy to address heterogeneity within tumors and the microenvironment and to determine the presence of blood vessels.

II. MATERIALS AND METHODS

A. Mouse tissue samples and preparation

The *pIns-c-MycER^{TAM}/p53$^{-/-}$* Myc-inducible mouse model was used to generate pancreatic β cell tumors.[21] In this model, the *c-Myc* gene (hereafter referred to as Myc) is regulated by an insulin promoter and generates a chimeric mutant estrogen receptor fused to the C-terminus of the Myc protein.[22] The presence of this fusion allows for Myc induction using tamoxifen injection, and the insulin promoter provides tissue specific expression in pancreatic β-cells.[4,21] On induction of Myc, hyperplasia and vascularization of β-cell islets were evident by 6 days. After 6 days of Myc activation, pancreatic tissues were harvested and frozen in optimal cutting temperature (OCT) compound. Control pancreas samples were harvested from *p53$^{-/-}$* mice, which had also been injected with tamoxifen for 6 days.[21] Four-micrometer thick cryosections were used for hematoxylin and eosin (H&E) staining or for ToF-SIMS analysis. Since the cryosection analyzed by ToF-SIMS is mounted directly onto a silicon wafer, H&E images of the adjacent tissue sections provide a reference to guide identification and selection of neoplastic islets within the tissue.

B. Mass spectrometry imaging

All ToF-SIMS experiments were performed with an ION-TOF TOF.SIMS 5-100 instrument (ION-TOF GmbH, Münster, Germany) equipped with a liquid metal ion gun (LMIG) for analysis and an electron flood gun for charge neutralization. The LMIG was used to generate a pulsed 25 keV Bi_3^+ beam impacting the target at an angle of 45°. The Bi_3^+ beam was set in spectroscopy mode for high mass resolution (HMR) to acquire spectra and images in both polarities. The Bi_3^+ current was typically 0.13–0.15 pA. Target currents were measured before each data set using a Faraday cup. Large optical stitches of all tissues were produced by manually stitching images from the video camera within the ToF-SIMS before analysis. Optical stitch images were then used to aid in selecting ToF-SIMS analysis areas. For all data collection, HMR positive ion data were acquired followed immediately by HMR negative ion data on the same area. X and Y sample stage coordinates were saved in the software to ensure that data acquired were from the same region in both polarities. Mass resolution ($m/\Delta m$) for the $C_2H_3^+$ ion was greater than 4500. Positive ion spectra were calibrated to CH_3^+, $C_2H_3^+$, and $C_4H_5^+$. Negative ion spectra were calibrated to CH^-, OH^-, and C_2H^-. Spectra were acquired from 1 mm × 1 mm "patches" comprising twenty five or twenty four 200 μm × 200 μm "tiles" on each tissue. Each tile contains 256 × 256 pixels, giving the patches a total pixel count of 1280 × 1280 and a pixel size of 781 nm × 781 nm. The purpose of analyzing smaller areas is to capture the localized areas of the islet tumors and to image the entire sample, which can undergo sample degradation or lipid migration over time.[23] The Bi_3^+ dose was limited to $\leq 5.0 \times 10^{11}$ ions/cm^2 for each tile in both positive and negative ion modes, resulting in a total Bi_3^+ dose of $\leq 1.0 \times 10^{12}$ ions/cm^2 per tile so that the static limit would not be surpassed. SURFACELAB 6 software (ION-TOF GmbH, Münster, Germany) was used for all analyses. A total of three Myc and four control tissue sections were analyzed with each tissue having a minimum of three selected patches.

C. Sum harmonic generation

The multiphoton excitation fluorescence (MPEF) and SHG images were acquired with a scanning confocal multiphoton microscope (Olympus, FV1000 MPE BX61) with a 20× objective. The light source was a tunable laser (Spectra-Physics Mai Tai) with λ_{exc} at 910 nm and with bandpass filters at 495–540 nm for the MPEF channel and 420–460 nm for the SHG channel. The detectors were photon multipliers, located so that the SHG captures in backscattering mode and the MPEF in epifluorescence mode. All SHG experiments were performed on H&E stained slides.

D. Data analysis

PCA was applied to ToF-SIMS images and spectra data acquired from the tissues. The resulting scores and loadings were used to identify distinct molecular species responsible for the contrast seen within the score images, thus providing

a method to spatially identify correlated masses/molecules for further investigation.

Regions of exposed silicon substrate and OCT (e.g., holes or tears from cutting tissue and embedding medium surrounding the tissue section) were excluded from all analyses by applying a threshold to the pixels with an Si^+ signal, where m/z 27.9 was used to detect silicon and m/z 332.2 ($C_{14}H_{29}$, a fragment of the benzalkonium additive in OCT)[24] is used to detect OCT areas. PCA was performed using the NBTOOLBOX IMAGEGUI (Daniel Graham, NESAC/BIO, University of Washington), which operates within MATLAB (MathWorks, Natick, MA). Peaks were chosen that had a maximum intensity two times or more than that of the average background intensity. The spectra from all tissues were overlaid, and then peaks were manually selected and integrated to full width half max. A total peak list of 1017 and 1349 peaks were chosen from the positive and negative ion modes, respectively. Normalization was not applied to imported image patches; image data were preprocessed by Poisson scaling and mean centering before PCA.

A comparison of relative intensities was achieved by first selecting regions of interest (ROIs) of either islets or acinar tissue without vascularized areas and normalizing ions to the total ion counts. This resulted in a total of 23 Myc and 12 control islets. The acinar ROIs resulted in nine regions for Myc and ten for the control. Normalized ion counts from these ROIs were then compared using Welch's unpaired t-tests with p-value <0.05 chosen as statistically significant.

III. RESULTS AND DISCUSSION

A. Distinguishing tumor islets from the acinar tissue using imaging PCA

Determining the spatial distribution of distinct lipids and metabolic intermediates within Myc-induced β cell tumors and the acinar tissue surrounding these tumors can identify metabolic abnormalities related to Myc-induced cellular proliferation and signaling. This information may also provide insight into the metabolic cross talk occurring between these two environments.

PCA of ToF-SIMS image data resulted in a separation between the Myc-induced tumor and acinar tissue in both polarities in PC1, demonstrating that the largest amount of chemical variance was between these regions. Figure 1 shows positive polarity PCA data, which exhibits separation of tumor from the surrounding acinar tissue within the first principal component score images for the Myc tissue. The PC1 scores and loadings reveal the major differences in chemistries between the tumor [Fig. 1(a)] and acinar tissue [Fig. 1(b)]. PC1 positive loadings relating to the tumor are dominated by the salt or salt containing peaks, such as the potassium isotope at m/z 40.96 ($^{41}K^+$), $CNKNa^+$ (m/z 87.96), and CNK_2^+ (m/z 103.93). Molecular peaks of metabolic interest also found in the positive loadings were Fe^+ (m/z 55.94), histidine fragments ($C_5H_8N_3^+$, m/z 110.07), phenylalanine fragments ($C_8H_{10}N^+$, m/z 120.08), phosphatidylcholine fragments ($C_6H_{17}NPO_4^+$, $C_5H_{14}NPO_4Na^+$, $C_5H_{14}NPO_4K^+$, m/z

198.10, 206.06, 222.03), and heme fragments ($C_{29}H_{21}FeN_4^+$, $C_{29}H_{23}FeN_4^+$, $C_{30}H_{25}FeN_4^+$, $C_{34}H_{32}FeN_4O_4^+$, m/z 481.05, 483.08, 497.10, 616.18)[25,26] [Fig. 1(a)]. PC1 negative loadings indicated that the acinar tissue surrounding the tumor correlated with Mg^+ (m/z 23.98), small hydrocarbon fragments ($C_3H_5^+$, $C_4H_6^+$, $C_5H_7^+$, m/z 41.04, 54.05, 67.05), and choline ($C_5H_{14}NO^+$, m/z 104.11) [Fig. 1(b)].

Recent work using matrix assisted laser desorption mass spectrometry imaging to investigate how Myc overexpression affects lipid metabolism in lung cancer observed an increased K^+ associated with tumors and a higher proportion of potassiated lipids in tumor regions.[20] Calcium and ATP-sensitive K^+ ion channels at the cell surface membrane of pancreatic β cells control insulin secretion. In healthy β cells, the potassium ion channels are normally open allowing potassium to diffuse out of the cell, but when the metabolism of glucose produces ATP, the ATP-sensitive potassium ion channels close.[27] Deregulation of this channel as well as an increased extracellular K^+ associated with the tumor may account for the K^+ adducts observed in loadings that correlate to the tumor.

In contrast to the Myc pancreatic tissue, where differences between islet and acinar tissue were evident in the first PC scores, there was no evident difference for this first PC in the PCA scores of image data in controls. Instead, the control islet was typically observed in PC2 to PC3 scores and associated with collagenous and vasculature structures. This indicates that the chemical variance between the islet and the acinar tissue was much lower than what is exhibited in the Myc tissue.

Individual ToF-SIMS images of key fragments for both Myc and control are illustrated in Fig. 2. The H&E stained tissue slices show an outlined region of the tumor [Fig. 2(a)] and the control islet [Fig. 2(b)] that were identified at the Fred Hutchinson Cancer Research Center (Fig. 2). Fe^+, histidine, and heme fragments were all observed in localized spots within the tumor [Figs. 2(d)–2(f)]. The presence of these ions is indicative of blood or vasculature present within the tumor, as histidine is known to be found on hemoglobin and $pIns$-c-$MycER^{TAM}/p53^{-/-}$ islet tumors[21] produce highly hemorrhagic vasculature.[4] Unlike the Myc islet tumors, the control islets did not exhibit increased signals of Fe^+, histidine, phenylalanine, or heme fragments within the islet [Figs. 2(j)–2(l)]. However, the acinar tissue of the control islet correlated with Mg^+ as was observed in the Myc tissue, and this is illustrated in Figs. 2(b) and 2(h).

PCA of ToF-SIMS negative polarity image data also distinctly separated the Myc islet tumor from the remaining acinar tissue within the first PC [supplementary material, Fig. 3 (Ref. 71)]. The positive loadings associated with the tumor are dominated by ions CN^- and CNO^-, Cl^-, and C14:0 (m/z 26.00, 42.00, 34.96, 227.20), but higher mass lipid fragments such as vitamin E ($C_{29}H_{49}O_2^-$, m/z 429.38) and fragments of sphingomyelin (SM) (34:1) ($C_{36}H_{69}NO_6P^-$, $C_{38}H_{76}N_2O_6P^-$, m/z 642.51, 687.56) are also observed. The presence of myristic acid (C14:0, $C_{14}H_{27}O_2^-$) localized within the tumor, not previously
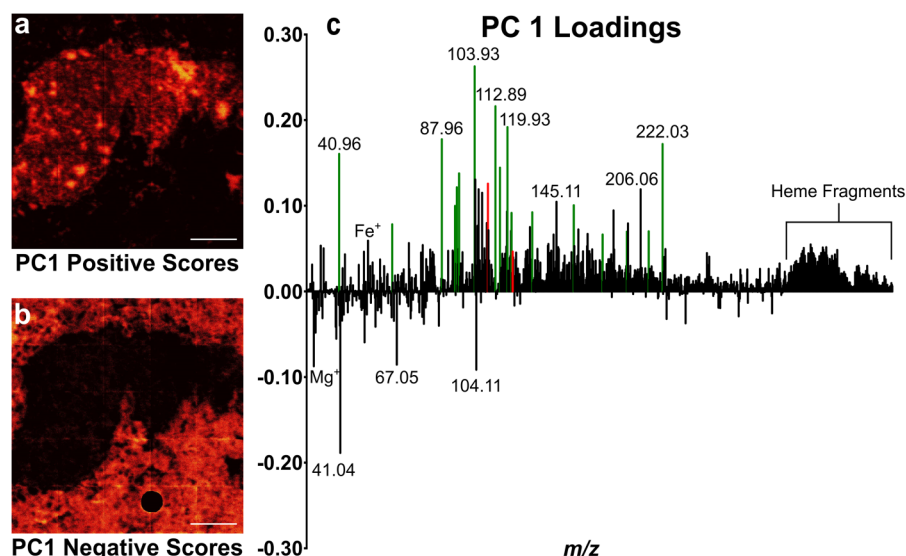
FIG. 1. Positive polarity PCA of ToF-SIMS image of Myc tissue region after removal of substrate/embedding medium signal. (a) PC1 positive score image displaying the Myc islet tumor. (b) PC1 negative score image displaying the acinar tissues. (c) PC1 loading plot displaying the chemical species that correspond to the score images. Key potassiated masses are colored green, histidine and phenylalanine are colored red, and masses corresponding to heme fragments are labeled. Scale bar is 200 μm.

documented in Myc-induced tumor lipid imaging work to date, shows a clear alteration in the lipid metabolism of Myc β cell tumors that is restricted to the tumor and does not arise in the surrounding acinar tissue. SM has been shown as a marker for the surface of β cells but is also an indicator of the functionality of the cells. Previous investigations observed that there is a correlation between insulin secretory capacity and the presence of SM in islets, where a higher level of SM correlates with a higher expression of insulin.[28] SM (34:1) and its fragments were also localized within the control islets [supplementary material, Fig. 2 (Ref. 71)].

In Myc tissues, the PC1 negative scores in the negative polarity were indicative of the acinar tissue around the tumor. The majority of the negative loadings in PC1 that are correlated with acinar tissue are consistent with salt adducts

as indicated by masses ending with 0.8–0.9. However, linoleic acid (C18:2, $C_{18}H_{31}O_2^-$, *m/z* 279.23) and a phosphoinositol fragment ($C_9H_{16}PO_9^-$, *m/z* 299.06) also had distinguishable negative loading values. The presence of linoleic acid outside of the islets can be explained by previous investigations showing stimulatory effects on insulin secretion from β cells.[29] The presence of linoleic acid was also observed in the tissue surrounding the control islets [supplementary material, Fig. 2 (Ref. 71)], and thus this is not a distinguishing feature of acinar tissue adjacent to Myc-induced β cell tumors.

Similarly to positive polarity PCA results, PCA of the negative polarity image data could not separate the control islets from the surrounding acinar tissue. Overall, the most distinct difference between Myc-induced islet tumors and
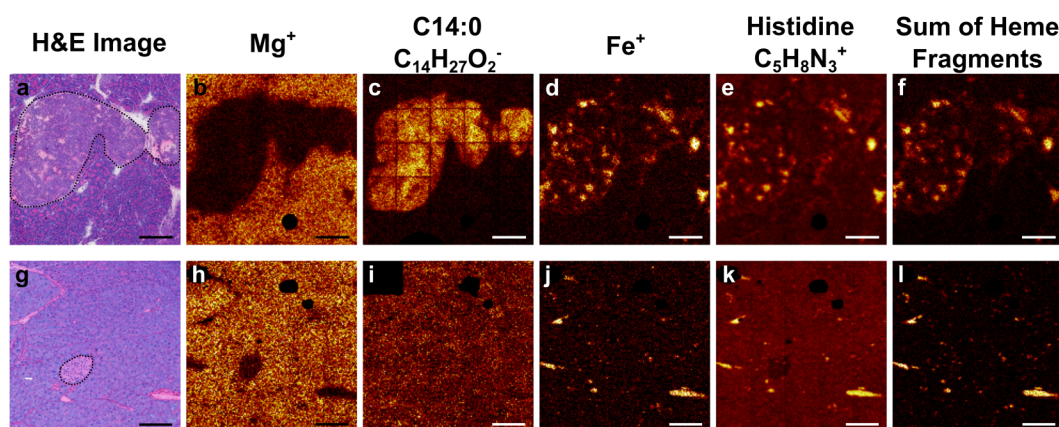

FIG. 2. ToF-SIMS images of metabolites observed in PCA across mouse pancreatic tissue sections. [Top, (a)–(f)] Myc tissues; [bottom, (g)–(l)] control pancreatic tissues. Islets are outlined with dashed lines in (a) and (g). Observed masses Mg^+ (*m/z* 23.98), C14:0, $C_{14}H_{27}O_2^-$ (*m/z* 227.20), Fe^+ (*m/z* 55.93), histidine, $C_5H_8N_3^+$ (*m/z* 110.07), sum of heme fragments $C_{29}H_{21}FeN_4^+$, $C_{29}H_{23}FeN_4^+$, $C_{30}H_{25}FeN_4^+$, $C_{34}H_{32}FeN_4O_4^+$ (*m/z* 481.05, 483.08, 497.10, 616.18). Signal from substrate and embedding medium were removed from images and can be seen as areas that are black and show no signal. Scale bar is 200 μm.

control islet in the negative data was the absence of C14:0 within the control islet [Figs. 2(c) and 2(i)]. Key ToF-SIMS images of masses observed in PCA can be seen in the supplementary material, Figs. 1 and 2.[71]

B. Tumor heterogeneity

Tumor heterogeneity is known to affect multiple properties such as responses to therapy, proliferation, and invasion.[30] Therefore, using ToF-SIMS to spatially characterize molecular intratumor heterogeneities may lead to the deconvolution of metabolic mechanisms occurring during tumor progression. The PCA score image shown in Fig. 1(a) and ToF-SIMS images in Figs. 2(d)–2(f) indicate areas of intratumor heterogeneity within the tumor. Using a method we previously developed and applied to breast tissue,[31] we separate out the tumor islet region by applying PCA to the spectra from pixels with positive scores on PC1, as shown in Fig. 1(a). Utilizing this method provides a direct characterization of the chemical variation occurring spatially within the tumor observed in both Figs. 1 and 2. These results are shown in Fig. 3 for the positive polarity and in the supplementary material, Fig. 4 (Ref. 71) for the negative polarity.

The positive polarity results separated the high intensity regions within the tumor in PC1 positive scores as shown in Fig. 3(a). The positive loadings [Fig. 3(c)] associated with the high intensity regions showed loadings of Fe^+, histidine fragments ($C_4H_6N_2^+$, $C_5H_8N_3^+$, $C_6H_5N_2O^+$, m/z 82.05^+, 110.07^+, 121.04^+), and heme fragments.[25,26] These fragments observed by PCA of these ROIs further provide chemical identification of these spatial locations and identified fragments that may potentially be related to vasculature and providing interior tumor characterization. As described above, masses that are associated with blood were present within the tumor, which may be providing visualization of early angiogenesis or blood vessel leakiness occurring within and around the tumor. Both angiogenesis and blood vessel leakiness occur frequently in tumors and provide both nutrients and oxygen that facilitate rapid tumor growth.[32,33]

The PC1 negative scores seen in Fig. 3(b) displayed the interior of the tumor and the corresponding negative loadings exhibited short chain hydrocarbon fragments, with most fragments associated with phosphatidylcholine, known to be the main lipid component within the cellular membrane. These chemical species are to be expected in the remaining areas of the tumor as these lipids make up the cellular components and membrane of the cells present in the islet.

The negative polarity PCA results also displayed separation of the high intensity regions from the remainder of the tumor in PC1 [supplementary material, Fig. 4 (Ref. 71)]. The positive scores displayed the tumor interior and the positive loadings exhibited fatty acids (C14:0, C16:0, $C_{16}H_{31}O_2^-$, C18:1, $C_{18}H_{33}O_2^-$, and C18:0, $C_{18}H_{35}O_2^-$, m/z 227.20, 255.23, 281.25, 283.26, respectively). All the fatty acids present within the islet tumor, besides C14:0, have been shown to be fragments of larger lipids in viable tumors and tumor tissues.[12,20,34]

The negative polarity PC1 negative scores, which correlate to the high intensity areas, displayed high loadings of CN^- and CNO^-. These molecular fragments are typically indicative of proteins or amino acids. Additionally, m/z 107.94 is found in the negative loadings which has been reported to come from the $Fe(CN)_2^-$ ion from heme as well.[35] These data agree with what was observed in the positive polarity, as both the heme and histidine fragments contain CN^- and CNO^-.

C. Sum harmonic generation microscopy of tumors and blood vessels

Using SHG, we sought to determine if there was any ordered structure similar to vasculature at these high intensity regions observed with ToF-SIMS within tumor areas. SHG is restricted to molecules with a noncentrosymmetric organization and provides for detailed optical images of fibrillary collagen and has been shown to image mixtures of collagens I and III around blood vessels.[36] Figure 4 shows images of a Myc tissue area that has both a tumor with the high intensity regions and a blood vessel next to a tumor. The molecular signals associated with both what appear to be blood and vasculature are shown in the ToF-SIMS images [Figs. 4(b)–4(d)] and are localized in the same areas as seen in the H&E image [Fig. 4(a)]. The chemistry of the blood vessel region at a higher magnification with a ToF-SIMS overlay image is shown in Fig. 4(f), where Fe^+, histidine, and heme fragments in green exhibit signal from the blood vessel, while phosphocholine shown in red represents the islet tumor boundary, and Mg^+ in blue shows the acinar tissue outside the tumor. The blood vessel from Figs. 4(a) and 4(e) imaged by SHG can be seen in Fig. 4(g). The structure of collagen within the blood vessel can be observed in the SHG image represented by a falsely colored green. Merging the SHG fluorescence (green) with autofluorescence (red) from the tissue [Fig. 4(h)] provides contrast, showing red in the cellular regions and the yellow overlay where the blood vessel structure is located. The suspected blood or vasculature areas can easily be observed in the H&E image of the Myc islet tumor in Fig. 4(i). Comparing these areas from Fig. 4(i) to the ToF-SIMS overlay image of an adjacent section [Fig. 4(j)], it can be seen that Fe^+, histidine, and heme fragments (green) show similar localizations. It is evident from the SHG image in Fig. 4(k) that there is no collagen present that would suggest blood vessel structure within the tumor islet, and the small circular areas of fluorescence are tissue debris trapped within the H&E mounting medium resulting in the scattering of photons. This combination of techniques provides evidence that these high signal regions are not vasculature.

These data are consistent with previous results which showed that erythrocytes remained present in pancreatic islet tumors after the vascular system was emptied and perfused with fixative solution due to defective blood vessel linings.[33] Some of these remaining red blood cells would form discrete blood lakes. However, further examination of the blood lakes showed that they were lined with tumor cells and showed no
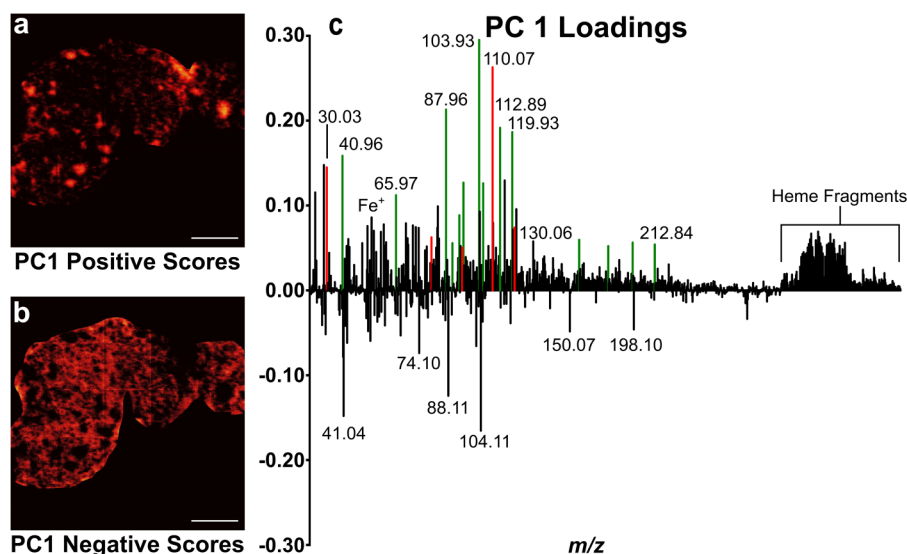
FIG. 3. Positive polarity PCA of ToF-SIMS image of the Myc islet tumor ROI. (a) PC1 positive score image displaying the high intensity regions within the Myc islet tumor. (b) PC1 negative score image displaying the tumor interior. (c) PC1 loading plot displaying the chemical species that correspond to the score images. Key potassiated masses are colored green, histidine fragments are colored red, and masses corresponding to heme fragments are labeled. Scale bar is 200 μm.
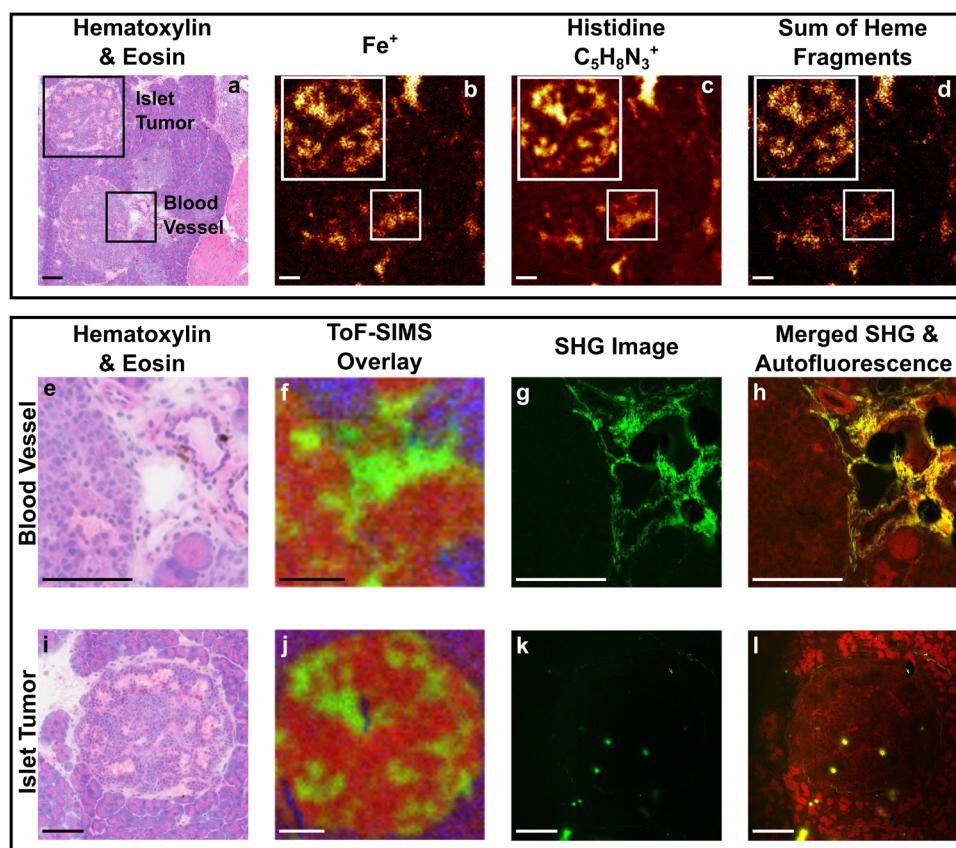

FIG. 4. H&E, ToF-SIMS, and SHG images of vasculature and blood lakes. Top row: (a) H&E of Myc tissue section containing a tumor with both blood lakes and blood vessels; [(b)–(d)] ToF-SIMS images of adjacent tissue section showing fragments related to blood lakes and vasculature. [Heme fragments shown in (d) are $C_{29}H_{21}FeN_4^+$, $C_{29}H_{23}FeN_4^+$, $C_{30}H_{25}FeN_4^+$, $C_{34}H_{32}FeN_4O_4^+$ (*m/z* 481.05, 483.08, 497.10, 616.18)]. Middle row: [(e)–(h)] the blood vessel region magnified. Bottom row: [(i)–(l)] the islet tumor region magnified. [(i) and (j)] A ToF-SIMS RGB overlay of red denoting the tumor (phosphocholine fragment, $C_5H_{14}NPO_4Na^+$, *m/z* 206.06), green denoting blood lakes or vasculature (sum of Fe^+, histidine, and heme fragments listed above), and blue denoting surrounding tissue (Mg^+, *m/z* 23.98). [(g) and (k)] Green colored fluorescence images acquired from SHG, where (g) shows the structure of the collagen lining the blood vessel and (k) shows scattering from debris but no SHG signal within the tumor. [(h) and (j)] The merged SHG and autofluorescence acquired using SHG, where the red represents autofluorescence occurring from the surrounding H&E stained cells. Scale bar is 100 μm.

evidence of direct connection to the blood stream. Further H&E and SHG images of blood lakes can be observed in the supplementary material, Fig. 5.[71]

D. Molecular differences between Myc tumor and control pancreatic tissue

To accurately associate changes occurring between the tumor microenvironment present in the Myc tissues, vasculature was removed from the data set and all peaks within the whole mass range were used for a complete comparison against the control tissues. The tissues were separated into two ROIs, the islets and the surrounding acinar tissue, and the peak intensities in the spectra for each region were compared between the Myc and control pancreatic sections. Using Welch's *t* test, all peaks were tested and compared and it was found that there were significant changes to the amino acid, nucleotides, and lipid content between the tissues. Tables I–III show the percentage change of biomolecules present in Myc and control islets and surrounding acinar tissue in both positive and negative polarities.

Amino acids and carnitines were found to have an increased normalized intensity while monoacylglycerides

(MAGs) and diacylglycerides (DAGs) decreased within the Myc islets compared with the control. The largest changes were observed in the histidine fragment $C_5H_8N_3^+$ (*m/z* 110.07) with a 2-fold increase in intensity, heme fragments with an approximately 2.5–3-fold increase in intensity, and Fe^+ with a 1.5-fold increase in intensity in the Myc islets due to the presence of blood lakes. Serine ($C_2H_6NO^+$, *m/z* 60.05) exhibited an approximate 40% increase in intensity in the Myc islets. Other key amino acid fragments such as methionine ($C_2H_5S^+$, *m/z* 61.01), phenylalanine ($C_9H_8O^+$, *m/z* 132.05), and tryptophan ($C_{11}H_8NO^+$, *m/z* 170.07) showed an approximate increase of 20%–25%. Many other amino acids exhibited a small increase between approximately 10% and 18% and are listed in Table I. There was a decrease of MAGs and DAGs within Myc islets as seen with MAG (18:2), MAG (18:1), MAG (18:0) (*m/z* 337.29, 339.29, 341.31), DAG (36:2), and DAG (36:1) (*m/z* 603.59 and 605.63), yet long-chain fully saturated PC (30:0) (*m/z* 706.55) and PC (32:1) (*m/z* 732.55) were elevated by 105% and 44%, respectively. However, PC (34:1) (*m/z* 760.59) and its potassiated [PC (34:1) + K, *m/z* 798.55] adduct decreased by approximately 40%. Palmitoylcarnitine (*m/z* 400.35), which facilitates the transfer of long-chain fatty acids from

TABLE I. Comparison of biomolecules identified in positive polarity for Myc islets and control islets. All results are statistically significant with a value of $p < 0.05$ according to *t* test with Welch's correction.

Description	Formula	Measured *m/z*	Myc islets mean ($\times 10^{-4}$)	Control islets mean ($\times 10^{-4}$)	Percent difference
Heme fragment	$C_{29}H_{21}FeN_4$	481.05	0.183 ± 0.094	0.047 ± 0.021	291.2
Heme fragment	$C_{29}H_{23}FeN_4$	483.08	0.207 ± 0.108	0.053 ± 0.027	287.0
Heme fragment	$C_{30}H_{25}FeN_4$	497.10	0.181 ± 0.088	0.052 ± 0.019	250.7
Iron	Fe	55.93	0.396 ± 0.147	0.160 ± 0.030	147.5
PC (30:0)	$C_{38}H_{77}NO_8P$	706.53	0.042 ± 0.012	0.021 ± 0.007	104.8
Histidine	$C_5H_8N_3$	110.07	6.09 ± 1.81	3.10 ± 1.00	96.8
Palmitoylcarnitine	$C_{23}H_{46}NO_4$	400.35	0.079 ± 0.019	0.054 ± 0.025	47.5
PC (32:1)	$C_{40}H_{79}NO_8P$	732.55	0.036 ± 0.012	0.025 ± 0.010	43.7
Serine	C_2H_6NO	60.045	3.50 ± 0.557	2.52 ± 0.612	38.8
PC (30:0) + K	$C_{38}H_{77}NO_8PK$	744.50	0.057 ± 0.017	0.044 ± 0.020	30.2
Phenylalanine	C_9H_8O	132.05	0.575 ± 0.071	0.453 ± 0.053	26.9
Carnitine	$C_7H_{16}NO_3$	162.11	0.226 ± 0.017	0.181 ± 0.017	24.5
Tryptophan	$C_{11}H_8NO$	170.06	0.667 ± 0.081	0.552 ± 0.087	20.7
Methionine	C_2H_5S	61.01	1.70 ± 0.328	1.41 ± 0.390	20.6
Glycine	C_3H_6NO	72.04	3.15 ± 0.244	2.69 ± 0.289	17.3
Glycine	CH_4N	30.03	36.5 ± 5.10	32.1 ± 4.84	15.6
Arginine	CH_5N_3	59.05	8.63 ± 1.55	7.49 ± 1.27	15.2
Arginine	$C_4H_{10}N_3$	100.09	2.36 ± 0.296	2.06 ± 0.341	14.7
Tyrosine	$C_8H_{10}NO$	136.08	1.35 ± 0.17	1.19 ± 0.210	13.2
Glutamine	C_4H_6NO	84.05	5.98 ± 0.880	5.29 ± 1.03	13.1
Threonine	C_4H_5O	69.04	9.50 ± 1.090	8.40 ± 1.06	13.0
Valine	C_5H_7O	83.05	7.47 ± 0.544	6.67 ± 0.501	12.0
Tyrosine	C_7H_7O	107.05	2.76 ± 0.266	2.50 ± 0.254	10.5
DAG (36:1)	$C_{39}H_{73}O_4$	605.55	0.035 ± 0.010	0.048 ± 0.019	−26.8
DAG (36:2)	$C_{39}H_{71}O_4$	603.54	0.035 ± 0.009	0.049 ± 0.021	−29.7
MAG (18:0)	$C_{21}H_{41}O_3$	341.30	0.063 ± 0.008	0.091 ± 0.016	−31.5
MAG (18:2)	$C_{21}H_{37}O_3$	337.27	0.054 ± 0.008	0.083 ± 0.022	−34.0
MAG (18:1)	$C_{21}H_{39}O_3$	339.29	0.061 ± 0.010	0.093 ± 0.028	−34.7
PC (34:1) + K	$C_{42}H_{82}NO_8PK$	798.54	0.064 ± 0.029	0.107 ± 0.060	−39.5
PC (34:1)	$C_{42}H_{83}NO_8P$	760.57	0.081 ± 0.039	0.134 ± 0.086	−40.1

TABLE II. Comparison of biomolecules identified in the negative polarity for Myc islets and control islets. All results are statistically significant with a value of $p < 0.05$ according to t test with Welch's correction.

Description	Formula	Measured m/z	Myc islets mean ($\times 10^{-4}$)	Control islets mean ($\times 10^{-4}$)	Percent difference
Myristic acid; 14:0	$C_{14}H_{27}O_2$	227.20	2.54 ± 0.762	0.58 ± 0.129	341.0
Adenine	$C_5H_4N_5$	134.05	7.10 ± 2.22	5.36 ± 1.55	32.3
Guanine	$C_5H_3N_5$	133.04	1.59 ± 0.417	1.30 ± 0.285	22.6
Thymine	$C_5H_5N_2O_2$	125.03	7.66 ± 0.811	7.00 ± 0.963	9.4
Pyruvic acid	$C_3H_4O_3$	87.01	9.81 ± 0.332	10.6 ± 0.974	-7.9
Palmitic acid; 16:0	$C_{16}H_{31}O_2$	255.23	21.6 ± 3.73	24.8 ± 4.55	-12.7
FA (24:0)	$C_{24}H_{47}O_2$	367.35	0.054 ± 0.005	0.063 ± 0.013	-14.1
FA (C22:4)	$C_{22}H_{35}O_2$	331.26	0.127 ± 0.019	0.153 ± 0.019	-17.3
Eicosenoic acid; 20:1	$C_{20}H_{37}O_2$	309.28	0.268 ± 0.044	0.329 ± 0.052	-18.4
FA (C24:1)	$C_{24}H_{45}O_2$	365.34	0.076 ± 0.007	0.095 ± 0.014	-19.3
SM (34:1)	$C_{37}H_{75}N_2O_6P$	673.51	0.096 ± 0.020	0.123 ± 0.032	-21.3
SM (34:1)	$C_{40}H_{80}N_2O_6P$	715.58	0.070 ± 0.018	0.092 ± 0.031	-24.0
SM (34:1)	$C_{36}H_{69}NO_6P$	642.50	0.441 ± 0.121	0.584 ± 0.181	-24.6
SM (34:1)	$C_{34}H_{67}NO_6P$	616.48	0.265 ± 0.064	0.355 ± 0.112	-25.4
FA (C22:5)	$C_{22}H_{33}O_2$	329.24	0.123 ± 0.017	0.175 ± 0.035	-29.6
FA (C22:6)	$C_{22}H_{31}O_2$	327.23	0.110 ± 0.013	0.162 ± 0.035	-32.3
Eicosapentaenoic acid; 20:5	$C_{20}H_{29}O_2$	301.22	0.149 ± 0.032	0.243 ± 0.058	-38.8
Eicosadienoic acid; 20:2	$C_{20}H_{35}O_2$	307.26	0.288 ± 0.051	0.523 ± 0.125	-44.9
Stearic acid; 18:0	$C_{18}H_{35}O_2$	283.26	8.27 ± 1.57	15.0 ± 2.52	-45.0
Vitamin E	$C_{29}H_{49}O_2$	429.37	0.392 ± 0.134	0.719 ± 0.228	-45.4
Eicosatrienoic acid; 20:3	$C_{20}H_{33}O_2$	305.25	0.414 ± 0.080	0.776 ± 0.161	-46.6
C18:3	$C_{18}H_{39}O_2$	277.22	0.275 ± 0.043	0.540 ± 0.105	-49.0
Oleic acid; 18:1	$C_{18}H_{33}O_2$	281.25	6.08 ± 1.54	12.3 ± 3.13	-50.6
PE (38:4)	$C_{43}H_{77}NO_8P$	766.55	0.029 ± 0.007	0.062 ± 0.023	-53.8
Arachidonic acid; 20:4	$C_{20}H_{31}O_2$	303.23	0.584 ± 0.161	1.33 ± 0.473	-56.1
PE (38:4)	$C_{43}H_{77}NO_7P$	750.54	0.029 ± 0.007	0.068 ± 0.028	-56.6
PE (38:3)	$C_{43}H_{79}NO_7P$	752.57	0.030 ± 0.008	0.087 ± 0.034	-65.9
Linoleic acid; 18:2	$C_{18}H_{31}O_2$	279.23	1.78 ± 0.459	5.83 ± 1.86	-69.5

TABLE III. Comparison of biomolecules identified in both negative and positive polarities for the surrounding acinar tissue of Myc and control of Myc islets vs control islets. All results are statistically significant with a value of $p < 0.05$ according to t test with Welch's correction.

Description	Formula	Measured m/z	Myc acinar mean ($\times 10^{-4}$)	Control acinar mean ($\times 10^{-4}$)	Percent difference
Positive polarity					
Palmitoylcarnitine	$C_{23}H_{46}NO_4$	400.35	0.062 ± 0.013	0.046 ± 0.011	36.6
Iron	Fe	55.93	0.174 ± 0.021	0.145 ± 0.009	20.2
Alanine/cysteine	C_2H_6N	44.05	85.7 ± 3.02	93.7 ± 7.01	-8.6
Tryptophan	$C_{11}H_8NO$	170.06	0.712 ± 0.039	0.807 ± 0.101	-11.7
Arginine	$C_4H_{10}N_3$	100.09	2.49 ± 0.292	2.90 ± 0.428	-14.0
Glutamine	C_4H_6NO	84.05	6.11 ± 0.917	7.11 ± 1.11	-14.1
Methionine	C_2H_5S	61.01	1.87 ± 0.337	2.29 ± 0.473	-18.5
Negative polarity					
Thymine	$C_5H_5N_2O_2$	125.04	6.27 ± 0.614	7.04 ± 0.724	-11.0
Guanine	$C_5H_4N_5O$	150.04	3.74 ± 0.555	4.39 ± 0.657	-14.9
GPGro headgroup	$C_6H_{12}O_6P$	211.04	0.507 ± 0.034	0.577 ± 0.057	-12.2
Palmitic acid; 16:0	$C_{16}H_{31}O_2$	255.23	21.4 ± 5.80	28.4 ± 7.12	-24.5
Adenosine-5-phosphate	$C_{10}H_{13}N_5O_7P$	346.06	0.382 ± 0.085	0.524 ± 0.152	-24.7
SM (34:1)	$C_{38}H_{76}N_2O_6P$	687.55	0.097 ± 0.011	0.128 ± 0.030	-26.0
Eicosadienoic acid; 20:2	$C_{20}H_{35}O_2$	307.26	0.093 ± 0.024	0.129 ± 0.042	-27.2
SM (34:1)	$C_{34}H_{67}NO_6P$	616.48	0.055 ± 0.018	0.083 ± 0.024	-28.0
SM (34:1)	$C_{38}H_{74}N_2O_6P$	673.51	0.121 ± 0.034	0.164 ± 0.051	-33.4
SM (34:1)	$C_{40}H_{80}N_2O_6P$	715.58	0.032 ± 0.008	0.049 ± 0.019	-34.9
PE (38:4)	$C_{43}H_{77}NO_7P$	750.54	0.030 ± 0.007	0.047 ± 0.022	-36.5
PE (38:3)	$C_{43}H_{79}NO_7P$	752.57	0.031 ± 0.008	0.051 ± 0.023	-38.7

the cytoplasm into the mitochondria during the oxidation of fatty acids, showed an increase of nearly 50% within Myc islets.

Myc islets showed over a threefold increase in myristic acid (C14:0, *m/z* 227.20) as shown in Table II. Increases of approximately 30% and 20% were observed in adenine ($C_5H_4N_5^-$, *m/z* 134.048) and guanine ($C_5H_3N_5^-$, *m/z* 133.04), respectively, and likely reflect nucleotide biosynthesis within the tumor. Myc islets showed an 85% decrease in cholesterol sulfate compared to control islets. Phophatidylethanolamine (PE) (38:4) and PE (38:3) (*m/z* 750.55, 752.60) also exhibited a decrease in Myc islets of more than half of the intensity observed in the control. Fatty acids such as arachidonic acid (AA, C20:4, *m/z* 303.24), linolenic acid (C18:3, *m/z* 277.23), oleic acid (C18:1, *m/z* 281.25), stearic acid (C18:0, *m/z* 283.26), eicosapentaenoic acid (C20:5, *m/z* 301.22), eicosatrienoic acid (C20:3, *m/z* 305.26), and eicosadienoic acid (C20:2, *m/z* 307.27) were all decreased in the Myc islets compared with the control with decreases ranging from approximately 40% to 55%. SM (34:1) characteristic fragments were also decreased by 20%–25% in Myc islets.

The acinar tissue surrounding the islets in both the Myc and control tissues presented less variation of biomolecules between tissue types than what was observed between islets. In the positive polarity, the largest changes were observed in palmitoylcarnitine which had a 37% increase in Myc tissue and iron with a 20% increase. In contrast, methionine (fragment $C_2H_5S^+$, *m/z* 61.01) was decreased by 19% in the Myc versus control acinar tissue. All other amino acids that showed a statistically significant difference ($p \leq 0.05$) between the normalized intensity means in the acinar tissue, exhibiting decreases ranging from 8% to 14%, are listed in Table III.

The Myc acinar tissue showed decreased intensities in all major biomolecules when compared with the control acinar tissue, with large decreases observed in all lipids except C14:0. PE (38:4) and PE (38:3) exhibited the largest decreases of 37% and 39%, respectively, within the Myc surrounding acinar tissue. SM (34:1) fragments all showed a consistent decrease ranging from 26% to 35%. In addition, smaller fatty acid fragments such as eicosadienoic acid (20:2) and palmitic acid (C16:0, *m/z* 255.23) demonstrated a decrease of 25%–27%. Adenosine monophosphate (AMP) ($C_{10}H_{13}N_5O7P^-$, *m/z* 346.06), a possible metabolite from the cyclic-AMP or hydrolysis of adenosine-diphosphate, was found to be 25% lower in Myc-surrounding acinar tissue. Other nucleotides such as thymine and guanine were also found to be slightly decreased in the Myc-surrounding acinar tissue by 11%–15%.

E. Discussion

Our analyses provide evidence of significant metabolic changes occurring within Myc-driven β cell tumors and the surrounding tissue, which demonstrates a proof-of-concept for utilizing ToF-SIMS to identify large-scale changes that occur in tumor and stromal cell metabolism during tumorigenesis. The specific alterations of significance include the *de novo* synthesis of fatty acids such as C14:0 and PC30:0, the increase in palmitoylcarnitine in the tumor and acinar tissue surrounding it, the increase in nucleotides, and the increase in amino acids within the tumor but depletion of amino acids within the acinar tissue.

Metabolites with high signal intensity within tumors included carnitine and palmitoylcarnitine and suggest increased fatty acid oxidation, as both are involved in transporting fatty acids across the mitochondrial membrane for oxidation and energy generation. The increase in palmitoylcarnitine and decrease in palmitate (C16:0) in Myc acinar tissue suggest that the tumor may also engage mechanisms to deplete palmitate from the surrounding environment to satisfy the high metabolic demands of tumor growth.

Metabolites increased in Myc acinar tissue include AMP and these levels may be influenced by Myc expression in the islet tumor. Myc overexpression is reported to deplete ATP, resulting in the activation of AMP-activated protein kinase (AMPK), a key protein for regulating cellular energy.[37] AMPK is switched on by the rise in the AMP:ATP ratio, which can either result from cellular stresses occurring with depletion of ATP (e.g., hypoxia or glucose deprivation) or stresses that increase ATP consumption (e.g., excessive cell growth), which are common occurrences in tumor cells.[38] AMPK activation inhibits biosynthetic pathways related to fatty acid and cholesterol synthesis while increasing catabolism.[39] This would agree with our data as we observed an increase in palmitoylcarnitine, which facilitates fatty acid oxidation, in both the Myc islets and acinar tissue surrounding the tumor. Together these data further support the hypothesis that the high energy demands of the Myc β cell tumor impact the metabolism of the surrounding cells and tissue, thereby providing a conducive tumor-promoting microenvironment.

The observed decrease in SM within the Myc islets is an indicator that the β cells are losing their capacity to produce insulin as there is a direct correlation between insulin secretory capacity and SM presence in islets.[28] SM synthases 1 and 2 have critical roles in allowing insulin vesicle release from Golgi cisterna and their inhibition repressed insulin secretion.[40] The decrease in β cell function could also be indicative of cellular dedifferentiation. According to Ischenko *et al.*, Myc is crucial for inducing the transformation from tumor cells to cancer stem cells.[41] Furthermore, activation of Myc in pancreatic β cells precipitates an acute loss of insulin production capacity with genes related to insulin production and other β cell lineage markers reduced significantly after 72 h, indicating a loss of β cell differentiation.[42] In addition, other research has shown that genome reprogramming and dedifferentiation are important early steps in pancreatic ductal adenocarcinoma tumor initiation and progression.[43–45] The decrease in SM found in the Myc acinar tissue may, in contrast, possibly be linked to AMPK activation and the inhibition of complex fatty acid synthesis resulting in shuttling of fatty acids to the tumor.

Lipids altered in Myc β cell tumors include increases in the short chain, fully saturated fatty acid, C14:0, and is likely a product of Myc-induced *de novo* fatty acid synthesis from glucose and/or possibly from glutamine via reverse carboxylation.[46] This would require overriding the AMPK block on synthesis outlined above but is consistent with previous studies demonstrating that Myc increases the gene expression profile for fatty acid synthesis and can also increase the profile of certain lipids in different cell types.[11,34,47,48] Evaluating the status of other lipid entities, the decreased intensity of AA (20:4) in the Myc islets is notable, as other groups have found its levels to be increased in Myc-activated tissues, such as the lung adenocarcinoma and lymphoma tissue.[20,34] In these models, increased AA is likely linked to production of eicosanoids, which regulate the inflammatory response and are implicated in cancer progression.[49–51] However, in pancreatic β cells arachidonic acid stimulates insulin secretion and its production requires DAG and MAG lipases[52] and a supply of MAG and DAG. In the Myc β cell tumors, the drop in AA is correlated with reduction in MAG and DAG fragments with similar decreases ranging from 27% to 35% and providing further evidence of loss of function and the potential dedifferentiation of β cells.

Phospholipids PC (30:0) and PC (30:0) + K$^+$ were increased in the Myc islets, and this is consistent with the high demand for membrane lipids generated in a rapidly growing tumor and possibly facilitated by the $p53^{-/-}$ status of these tumors.[53] These PC increases could explain the potential fate of the highly increased short chain fatty acid, C14:0, as the composition of PC (30:0) is most likely C14:0 and C16:0.

The increase in a wide array of amino acids within the Myc islets is a potential marker of enhanced cellular growth and proliferation, as growing tumors require large amounts of energy and building blocks for the construction of new cellular components.[38,54] The approximate 39% increase in serine observed in the Myc islets compared with the control islets is in agreement with prior investigations of cancer metabolism, as the serine biosynthetic pathway represents a critical change in glucose metabolism contributing to tumor growth and cellular reprogramming.[55–57] 3-phosphoglycerate, a glycolytic intermediate, is converted to serine through a series of enzymes, a number of which are upregulated in Myc-induced liver tumors (PHGDH, PSAT1, and PSPH),[58] and Myc activation of serine biosynthesis aids cancer progression under nutrient deprived conditions.[59] Further serine metabolism by serine hydroxymethyltransferase, also Myc-regulated,[60] leads to the production of glycine, which also increased by approximately 17% within Myc islets. Serine and glycine are precursors used in the folate cycle, which in turn provides precursors to generate methionine,[61] and methionine was increased within the Myc islets and decreased in the surrounding acinar tissue. Methionine adenosyltransferase (MAT), an enzyme that catalyzes the first step in methionine metabolism, has been associated with rapid growth and dedifferentiation of cells within the liver,[62,63] and methionine metabolism is deregulated in Myc-driven liver cancer.[59] The

role of methionine provides possible insight into the metabolic contribution to physiological changes occurring in our model, as the β cells within the Myc islets are showing signs of dedifferentiation as discussed above and are in a state of rapid growth. The depletion of methionine in the acinar tissue around the Myc islet is likely due to the high requirement of methionine needed for MAT and subsequent methyl donation within the tumor facilitating epigenetic changes associated with dedifferentiation, which requires gene silencing of dedicated tissue lineage markers.[64] Other amino acids increased in Myc islets include the essential amino acids phenylalanine and tyrosine. Previous studies have demonstrated that these two essential amino acids, both potentially transported by the Myc-regulated transporter Slc7a5,[65] are key contributors to primary tumor growth and metastasis.[66] These studies by Elstad *et al.* demonstrated that a diet that restricts phenylalanine and tyrosine resulted in longer survival and inhibition of primary tumor growth and metastasis in mice. Additional amino acids increased by 10%–15% in Myc β cell tumors include arginine, a provider of pivotal metabolic intermediates and essential for cancer cell growth,[67] valine, an essential amino acid with increased uptake in cancer cells,[68] and also threonine, which if combined with induction of threonine dehydrogenase would supplement tumor cell pools of glycine and acetyl CoA, contributing to *S*-adenosylmethionine synthesis, the abundance of which regulates histone methylation and cell fate.[69]

Finally, a counterintuitive finding was the increase in glutamine observed in the Myc islets, as other groups have noted that Myc overexpression drives glutamine catabolism rather than synthesis.[19,70] This increase in glutamine in the tumor may be derived from a combination of *de novo* synthesis and transport of glutamine from the surrounding cells as there is depletion of glutamine in Myc acinar cells. Glutamine is highly concentrated in the blood lakes present in Myc β-cell tumors, and these may act as a fuel source sink providing metabolites to the tumor.

IV. SUMMARY AND CONCLUSIONS

Imaging ToF-SIMS provides a new approach for imaging the tumor microenvironment and tumor heterogeneity, and our results demonstrate the potential to differentiate altered metabolic processes occurring within cancerous tissues. PCA of ToF-SIMS image data of pancreatic tissue containing β cell tumors revealed distinct chemical differences between the lipid and amino acid content within the tumor and surrounding tissue. Characterization of intratumor heterogeneity was successfully accomplished by selecting ROIs to separate the tumor region from the surrounding tissue and applying PCA to the ROI data. PCA of the tumor region allowed for chemical identification of spatial heterogeneity occurring within the tumor, showing the composition of blood lakes in discrete areas and the remaining biomolecules present within the tumor. The multimodal approach of ToF-SIMS images and SHG microscopy demonstrated that chemical and structural imaging modalities can correlate with each other in

defining the biological structures within tissue, such as blood vessels. Lastly, data interpretation using ROIs of ToF-SIMS images, peak intensity comparisons, and SHG provides a method to observe significant changes occurring within pancreatic *β* cell tumors and the surrounding tissue. Together these data collection and analysis methods demonstrate that imaging ToF-SIMS can provide biologically valuable chemical characterization of metabolites in tissues comprising the tumor and microenvironment at a high lateral resolution with low mass capabilities.

[1] T. L. Whiteside, Oncogene **27**, 5904 (2008).

[2] O. Tredan, C. M. Galmarini, K. Patel, and I. F. Tannock, J. Natl. Cancer Inst. **99**, 1441 (2007).

[3] A. Vazquez, J. J. Kamphorst, E. K. Markert, Z. T. Schug, S. Tardito, and E. Gottlieb, J. Cell Sci. **129**, 3367 (2016).

[4] A. Finch, J. Prescott, K. Shchors, A. Hunt, L. Soucek, T. B. Dansen, L. B. Swigart, and G. I. Evan, Cancer Cell **10**, 113 (2006).

[5] Z. E. Stine, Z. E. Walton, B. J. Altman, A. L. Hsieh, and C. V. Dang, Cancer Discov. **5**, 1024 (2015).

[6] D. R. Wise *et al.*, Proc. Natl. Acad. Sci. U.S.A. **105**, 18782 (2008).

[7] H. Zirath *et al.*, Proc. Natl. Acad. Sci. U.S.A. **110**, 10258 (2013).

[8] L. R. Edmunds *et al.*, J. Biol. Chem. **289**, 25382 (2014).

[9] F. Morrish and D. Hockenbery, Cold Spring Harb. Perspect. Med. **4**, a014225 (2014).

[10] F. Li *et al.*, Mol. Cell Biol. **25**, 6225 (2005).

[11] F. Morrish, J. Noonan, C. Perez-Olsen, P. R. Gafken, M. Fitzgibbon, J. Kelleher, M. VanGilst, and D. Hockenbery, J. Biol. Chem. **285**, 36267 (2010).

[12] K. Chughtai, L. Jiang, T. R. Greenwood, K. Glunde, and R. M. Heeren, J. Lipid Res. **54**, 333 (2013).

[13] M. A. Robinson, D. J. Graham, F. Morrish, D. Hockenbery, and L. J. Gamble, Biointerphases **11**, 02A303 (2015).

[14] M. K. Passarelli, C. F. Newman, P. S. Marshall, A. West, I. S. Gilmore, J. Bunch, M. R. Alexander, and C. T. Dollery, Anal. Chem. **87**, 6696 (2015).

[15] L. S. Eberlin, A. L. Dill, A. B. Costa, D. R. Ifa, L. Cheng, T. Masterson, M. Koch, T. L. Ratliff, and R. G. Cooks, Anal. Chem. **82**, 3430 (2010).

[16] B. Spengler, Anal. Chem. **87**, 64 (2015).

[17] B. Cillero-Pastor, G. Eijkel, A. Kiss, F. J. Blanco, and R. M. Heeren, Anal. Chem. **84**, 8909 (2012).

[18] J. Brison, M. A. Robinson, D. S. Benoit, S. Muramoto, P. S. Stayton, and D. G. Castner, Anal. Chem. **85**, 10869 (2013).

[19] E. H. Shroff *et al.*, Proc. Natl. Acad. Sci. U.S.A. **112**, 6539 (2015).

[20] Z. Hall, Z. Ament, C. H. Wilson, D. L. Burkhart, T. Ashmore, A. Koulman, T. Littlewood, G. I. Evan, and J. L. Griffin, Cancer Res. **76**, 4608 (2016).

[21] S. Pelengaris, M. Khan, and G. I. Evan, Cell **109**, 321 (2002).

[22] T. D. Littlewood, D. C. Hancock, P. S. Danielian, M. G. Parker, and G. I. Evan, Nucleic Acids Res. **23**, 1686 (1995).

[23] P. Sjövall, B. Johansson, and J. Lausmaa, Appl. Surf. Sci. **252**, 6966 (2006).

[24] L. J. Gamble, D. J. Graham, B. Bluestein, N. P. Whitehead, D. Hockenbery, F. Morrish, and P. Porter, Biointerphases **10**, 019008 (2015).

[25] V. Mazel, P. Richardin, D. Debois, D. Touboul, M. Cotte, A. Brunelle, P. Walter, and O. Laprevote, Anal. Chem. **79**, 9253 (2007).

[26] D. E. Greenwalt, Y. S. Goreva, S. M. Siljestrom, T. Rose, and R. E. Harbach, Proc. Natl. Acad. Sci. U.S.A. **110**, 18496 (2013).

[27] P. Petit and M. M. Loubatieres-Mariani, Fundam. Clin. Pharmacol. **6**, 123 (1992).

[28] A. Kavishwar and A. Moore, J. Histochem. Cytochem. **61**, 910 (2013).

[29] Y. Itoh *et al.*, Nature **422**, 173 (2003).

[30] R. Durrett, J. Foo, K. Leder, J. Mayberry, and F. Michor, Genetics **188**, 461 (2011).

[31] B. M. Bluestein, F. Morrish, D. Hockenbery, and L. J. Gamble, Microsc. Microanal. **21**, 2065 (2015).

[32] P. Carmeliet and R. K. Jain, Nature **407**, 249 (2000).

[33] H. Hashizume, P. Baluk, S. Morikawa, J. W. McLean, G. Thurston, S. Roberge, R. K. Jain, and D. M. McDonald, Am. J. Pathol. **156**, 1363 (2000).

[34] L. S. Eberlin, M. Gabay, A. C. Fan, A. M. Gouw, R. J. Tibshirani, D. W. Felsher, and R. N. Zare, Proc. Natl. Acad. Sci. U.S.A. **111**, 10450 (2014).

[35] J. Lindgren *et al.*, Sci. Rep. **7**, 13324 (2017).

[36] W. R. Zipfel, R. M. Williams, R. Christie, A. Y. Nikitin, B. T. Hyman, and W. W. Webb, Proc. Natl. Acad. Sci. U.S.A. **100**, 7075 (2003).

[37] L. R. Edmunds *et al.*, PLoS ONE **10**, e0134049 (2015).

[38] M. G. Vander Heiden, L. C. Cantley, and C. B. Thompson, Science **324**, 1029 (2009).

[39] S. M. Jeon, Exp. Mol. Med. **48**, e245 (2016).

[40] M. Subathra, A. Qureshi, and C. Luberto, PLoS ONE **6**, e23644 (2011).

[41] I. Ischenko, J. Zhi, U. M. Moll, A. Nemajerova, and O. Petrenko, Proc. Natl. Acad. Sci. U.S.A. **110**, 3937 (2013).

[42] S. C. Robson, L. Ward, H. Brown, H. Turner, E. Hunter, S. Pelengaris, and M. Khan, BMC Genomics **12**, 476 (2011).

[43] C. Guerra, A. J. Schuhmacher, M. Canamero, P. J. Grippo, L. Verdaguer, L. Perez-Gallego, P. Dubus, E. P. Sandgren, and M. Barbacid, Cancer Cell **11**, 291 (2007).

[44] S. Y. Gidekel Friedlander, G. C. Chu, E. L. Snyder, N. Girnius, G. Dibelius, D. Crowley, E. Vasile, R. A. DePinho, and T. Jacks, Cancer Cell **16**, 379 (2009).

[45] E. R. Lawlor, L. Soucek, L. Brown-Swigart, K. Shchors, C. U. Bialucha, and G. I. Evan, Cancer Res. **66**, 4591 (2006).

[46] M. Thai, S. K. Thaker, J. Feng, Y. Du, H. Hu, T. Ting Wu, T. G. Graeber, D. Braas, and H. R. Christofk, Nat. Commun. **6**, 8873 (2015).

[47] F. Morrish, N. Isern, M. Sadilek, M. Jeffrey, and D. M. Hockenbery, Oncogene **28**, 2485 (2009).

[48] L. R. Edmunds *et al.*, Oncotarget **7**, 30379 (2016).

[49] H. Harizi, J. B. Corcuff, and N. Gualde, Trends Mol. Med. **14**, 461 (2008).

[50] E. R. Greene, S. Huang, C. N. Serhan, and D. Panigrahy, Prostaglandins Other Lipid Mediat. **96**, 27 (2011).

[51] T. B. Angerer, Y. Magnusson, G. Landberg, and J. S. Fletcher, Anal. Chem. **88**, 11946 (2016).

[52] R. J. Konrad, C. D. Major, and B. A. Wolf, Biochemistry **33**, 13284 (2002).

[53] N. Mori, R. Delsite, K. Natarajan, M. Kulawiec, Z. M. Bhujwalla, and K. K. Singh, Mol. Imaging **3**, 319 (2004).

[54] C. V. Dang, Cold Spring Harb. Perspect. Med. **3**, a014217 (2013).

[55] I. Amelio, F. Cutruzzola, A. Antonov, M. Agostini, and G. Melino, Trends Biochem. Sci. **39**, 191 (2014).

[56] A. C. Newman and O. D. K. Maddocks, Trends Cell Biol. **27**, 645 (2017).

[57] M. Yang and K. H. Vousden, Nat. Rev. Cancer **16**, 650 (2016).

[58] A. Vazquez, E. K. Markert, and Z. N. Oltvai, PLoS ONE **6**, e25881 (2011).

[59] B. Anderton *et al.*, EMBO Rep. **18**, 569 (2017).

[60] M. A. Nikiforov, S. Chandriani, B. O'Connell, O. Petrenko, I. Kotenko, A. Beavis, J. M. Sedivy, and M. D. Cole, Mol. Cell Biol. **22**, 5793 (2002).

[61] J. W. Locasale, Nat. Rev. Cancer **13**, 572 (2013).

[62] J. Cai, Z. Mao, J. J. Hwang, and S. C. Lu, Cancer Res. **58**, 1444 (1998).

[63] Z. Z. Huang, Z. Mao, J. Cai, and S. C. Lu, Am. J. Physiol. **275**, G14 (1998).

[64] T. Chen and S. Y. Dent, Nat. Rev. Genet. **15**, 93 (2014).

[65] K. Hayashi, P. Jutabha, H. Endou, and N. Anzai, Oncol. Rep. **28**, 862 (2012).

[66] C. A. Elstad, G. G. Meadows, and R. M. Abdallah, Clin. Exp. Metastasis **8**, 393 (1990).

[67] D. Schechter, G. A. Bachmann, J. Vaitukaitis, D. Phillips, and D. Saperstein, Psychosom. Med. **51**, 173 (1989).

[68] V. E. Baracos and M. L. Mackenzie, J. Nutr. **136**, 237S (2006).

[69] N. Shyh-Chang *et al.*, Science **339**, 222 (2013).

[70] C. V. Dang, Cancer Res. **70**, 859 (2010).

[71] See supplementary material at https://doi.org/10.1116/1.5038574 for ToF-SIMS images for individual ions not shown in main text as well as extra PCA results and SHG images.

Lara Gamble: I was honored to be asked to submit an article to this special issue of Biointerphases. I have been working the field of surface characterization and modification for many years and have enjoyed being part of the growth and development of this field. I began my science career with a foundation in Chemistry (undergraduate degree in Chemistry from University of California, Santa Cruz and a Ph.D. in Physical Chemistry from the University of Washington). I have always had a strong interest in kinetics, catalysis and how surfaces play a key role in many chemical reactions. After my postdoc, I spent some time in industry at Zyomyx, Inc., a biotech startup in Fremont, CA and then at the Space Dynamics Laboratory (SDL) in Logon Utah. I am currently a Bioengineering Research Associate Professor at the University of Washington (UW) and the Co-Director of the long running National ESCA and Surface Analysis Center for Biomedical Problems (NESAC/BIO). I more recently also took on the role of Associate Director of the Molecular Analysis Facility (MAF) at the UW. My current scientific research interests include surface modification and characterization, biomaterials, biosensors, and molecular imaging in 2D and 3D.

I was asked to expand my biography with some words of advice or inspiration. I have been trying to define what to say and how best to be inspirational. We all play many roles in life. I am a daughter, sister, friend, wife, mother, employee, mentor, and the list goes on, but when I am asked to 'define' who I am that I bring with me to guide me in these roles we all fulfill in life, my first thought is always 'scientist'. In my mind, being a scientist is not a profession, but a way of life. I am a scientist because I love discovery and learning. I enjoy being with other people whose driving purpose is about learning and discovering the truth. Even if we leave the academic research 'grind', even if we leave an industrial research lab or a national lab, we will still be scientists because of the way we think, because of who we are. Our curiosity and learning will never stop. I try and remember that I am lucky to have this moment when I can do, as a profession, something that matches who I am and what I love. No matter what happens in the future, I have this moment. I try and remember to enjoy the present and not worry too much about the future.

We are all faced with challenges in our careers. When I think about advice, perhaps on how I overcome these hurdles in my career or my life, the only advice I can think of is what seems to work best for me when I hit hurdles. Recently, a friend pointed out that it is the unknown, the waiting, that causes the worry and stress. As one of my old officemates (when I was a postdoc) use to suggest, "Field the Ball". After asking what this meant (since I am not much of a baseball player) I found it means always moving towards the challenge before it comes to you. So, when faced with a challenge, I try to be proactive and tackle it head on because I know what I want from life. I advise moving towards the challenges, and not shying from them or waiting for them to be put in your path. Field the Ball.

Collaborators:

Blake Bluestein received his B.S. in Chemical Engineering from the University of New Mexico in 2011. He earned his Ph.D. from the NESAC/BIO at the University of Washington in 2017, where his project focused on imaging and analysis of cancerous tissues using ToF-SIMS. The primary goal of this work was to develop data analysis techniques that reveal significant metabolic events occurring within the tumor microenvironment, cancer metabolism, and aid in potential diagnosis and treatment efficacy. Blake is currently a Materials Analysis Engineer at Intel Corporation.

Daniel Graham received a B.S in Chemical Engineering from Brigham Young University and a Ph.D. in Bioengineering from the University of Washington. He is currently working as the NESAC/BIO Research Coordinator and a Senior Research Scientist in the department of Bioengineering at the University of Washington. Dan's research interests include 2D and 3D ToF-SIMS imaging of cells, tissues, and complex biomaterial surfaces, and development of software tools and methods for processing of chemical imaging data (both spectra and images). These tools were implemented in this work and aided in extracting relevant chemical information from the tumor microenvironment.

Dr. Fionnuala Morrish initially trained as a Plant Scientist but transitioned to Cancer research through fellowships in Medical Genetics and Cancer Biology. She currently holds a Staff Scientist position with the Fred Hutchinson Cancer Research Center, where she initiated studies on c-MYC's role as a regulator of central carbon metabolism. An interest in the contribution of metabolites from the tumor microenvironment to tumor aggressiveness led to collaborations with Dr. Gamble's group to study metabolic biomarkers for breast cancer and the current work on an inducible *in vivo* model of pancreatic β cell neoplasia.

Dr. David Hockenbery is a physician-scientist at Fred Hutchinson Cancer Research Center, specializing in gastroenterology. His research is focused on mitochondrial pathways of apoptosis, and the role of cellular metabolism in determination of cell fates, including apoptosis. Dr. Hockenbery received a B.S. in Chemical Engineering from the University of Rochester and an M.D. from Washington University in St. Louis. He completed residency in internal medicine at Johns Hopkins, where he served as Assistant Chief of Service. He pursued postdoctoral training with Dr. Stan Korsmeyer, one of pioneers in the Bcl-2 field, at Washington University.